nature astronomy

Article

https://doi.org/10.1038/s41550-025-02508-8

No magmatic driving force for Europan sea-floor volcanism

Received: 26 March 2024

Accepted: 17 February 2025

Published online: 24 March 2025

Check for updates

A. P. Green [1] ✉, C. M. Elder [1], M. T. Bland [2], P. J. Tackley [3] & P. K. Byrne [4]

The internal ocean of Jupiter's moon Europa is thought to be a prime candidate for hosting extraterrestrial life. Europa's silicate interior may contribute to habitability through the generation of reactants from hydrothermal activity, serpentinization or other geological processes occurring on or just below Europa's sea floor. However, silicates are thought to melt at depths >100 km in Europa's mantle, and it is unknown whether this magma can penetrate and travel through the moon's probably thick, brittle lithosphere to erupt at the sea floor. We combine previous approaches for modelling melt generation in the Europan interior and lithospheric dyke transport to show that Europan sea-floor volcanism is strongly inhibited by its lithosphere. The low stress state of the Europan interior hinders the ability of dykes to penetrate through the lithosphere. Should dykes form, they penetrate <5% of the 200–250-km-thick lithosphere. Low mantle melt fractions (3–5%) drive a sluggish pore-space magma flow, leading to dyke influxes 10,000 times lower than that necessary for sea-floor eruption. These results strongly indicate that models of Europan habitability reliant on present-day volcanism at its sea floor are implausible.

At the forefront of questions about Europa's habitability is how to maintain a stable oceanic biosphere in the present day without relying on photosynthesis[1–6]. Europa's outermost icy shell entirely blocks sunlight from the ocean, necessitating the development of sustained chemical disequilibrium in Europa's ocean from which cellular life may extract energy instead[1]. Such a biosphere requires a periodic geochemical source[5–8] of various oxidants and reactants[9–11], such as H_2, CH_4, CH_2O and H_2S (among others) to ensure that Europa avoids a state of 'thermodynamics-driven extinction'[5] by reaching a chemical equilibrium state.

Europa's structure may be well suited for generating and delivering these important reactants into the ocean. Its position inside Jupiter's plasma and radiation belts drives surface radiolysis, and the oxidants generated by this process could be delivered through the ice shell into the ocean. Although this delivery is far from assured, subduction-like processes[12,13] or direct shell–ocean exchange[14] may provide viable pathways, depending on the thickness and dynamic state of the shell[4,15]. Additionally, unlike larger ocean worlds, such as Ganymede and Titan, Europa's ocean is probably in direct contact with the underlying rocky interior, allowing for direct, low-temperature rock–water interactions, which may supply various important bioavailable heavy elements (such as Fe and Mg)[16] to any chemotrophs present.

Another crucial geochemical input stems from the possible presence of geothermally driven rock–water reactions at Europa's sea floor. Strong Jovian tides are known to heat Europa's interior[17,18]. These have been hypothesized to drive magmatism and possible sea-floor volcanism. Critically important reductants, such as H_2 and CH_4, could be produced by sea-floor volcanism or other geological processes such as hydrothermal vent activity[7] or serpentinization[8]. However, due to the position of the silicate interior—under approximately 100 km of water and ice, no direct observations of the sea floor or Europa's deep interior have yet been made. Therefore, although volcanism is often invoked in discussions of Europa's putative habitability, whether this process is actually occurring remains an open question.

In the absence of observational data, this question must be addressed by modelling. Recent whole-mantle modelling studies[9,10]

[1]Jet Propulsion Laboratory, California Institute of Technology, Pasadena, CA, USA. [2]US Geological Survey, Astrogeology Science Center, Flagstaff, AZ, USA. [3]Department of Earth and Planetary Sciences, ETH Zurich, Switzerland. [4]Department of Earth, Environmental, and Planetary Sciences, Washington University, St Louis, MO, USA. ✉e-mail: apgreen1515@gmail.com

https://doi.org/10.1038/s41550-025-02508-8

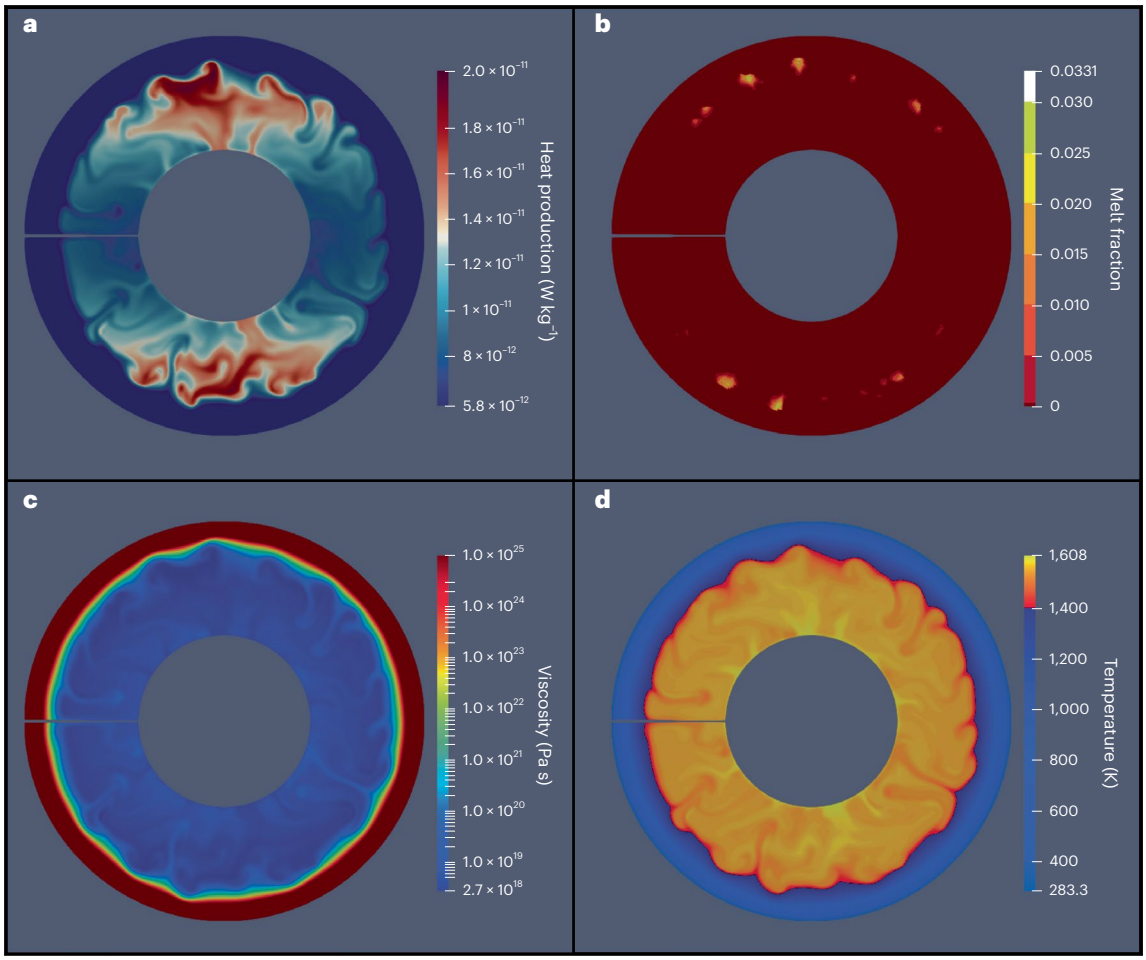

Fig. 1 | Illustration of the state of the reference model after 200 Myr of modelled time. a–d, The reference model features an 821-km-thick layer of peridotite undergoing thermal convection due to a combination of radiogenic and tidal heating. A full list of reference model parameters is given in Supplementary Table 1. **a**, Internal heat production in the model. **b**, Modelled melt fraction. When the temperature exceeds the local solidus (dependent on pressure), a partial melt will form. **c**, Material viscosity of the model. **d**, Material temperature. The colour scale is split into lithospheric temperatures ($T \leq 1{,}400$ K; blue) where the material is too rigid to participate in convection and sublithospheric temperatures ($T > 1{,}400$ K; orange-red) where active thermal convection occurs. Enlarged versions of each panel are shown as Supplementary Figs. 1–4.

have found that Europa's mantle is capable of producing melt, which is broadly supportive of Europan sea-floor volcanism. However, this melt is generated at depths of hundreds of kilometres and must then be transported to its sea floor for it to erupt. The primary obstacle in this process is the mantle lithosphere. Modelling has shown that the Europan mantle probably convects in the 'stagnant lid' regime[9,17], in which a thick, single-plate and essentially immobile lithosphere forms over a viscously flowing mantle[19,20]. In Europa's case, this lithosphere may reach thicknesses ranging from 100 to 400 km (ref. 9).

However, most mantle-scale modelling, if it includes magma generation and transport at all, tends to sidestep lithospheric melt transport by assuming that all melt is extracted or by applying simple criteria for eruption[9]. The lithospheric phase of melt transport often takes place on spatial and temporal scales much smaller than mantle geodynamic processes, and the two are, therefore, challenging to reconcile with modelling. When modelling a terrestrial planet, the existence of mantle melt extraction is not called into question due to extensive observations of past and present volcanism, making these approximations generally acceptable. Despite this, the development of magma plumbing systems in the lithosphere is a complex field of study in its own right[21–24], and that complexity should be accounted for when evaluating the potential for Europan sea-floor volcanism.

Two recent studies are illustrative of the modelling problems generated by these clashing spatio-temporal scales. Běhounková et al.[9] designed a 3D thermal evolution model of Europa's mantle and demonstrated that silicate melt can be generated throughout the moon's entire history. However, Běhounková et al.[9] assumed that all melt generated in their model is immediately extracted to the sea floor, ignoring melt migration through the mantle and the problem of lithospheric melt transport. On the other hand, Bland & Elder[11] focused entirely on Europa's lithosphere, developing a model of lithospheric dyke transport capable of identifying conditions supportive of Europan sea-floor volcanism. Missing from Bland and Elder's[11] model was consideration of mantle melt generation and accumulation. Without a way of determining the supply of mantle-generated magma to these lithospheric dykes, Bland & Elder[11] could not determine whether volcanism actually occurs, instead simply emphasizing that lithospheric transport may limit Europa's sea-floor volcanism.

Here, we combine the modelling approaches of Běhounková et al.[9] and Bland and Elder[11] with the convection simulation code StagYY[25] to provide a robust test of the plausibility of Europan sea-floor volcanism. First, we constructed a two-dimensional (2D) spherical model of Europa's mantle in StagYY[25], which was benchmarked to the present thermal conditions found by Běhounková et al.[9] (Fig. 1 and Supplementary Figs. 1–4; see Methods for model details). We then developed

https://doi.org/10.1038/s41550-025-02508-8

within StagYY a new melt-extraction routine based on the model of lithospheric dyke transport evaluated by Bland and Elder[11] (Supplementary Fig. 5; see Methods and Supplementary Discussion 1). StagYY simulates mantle convection with procedures for partial melt generation and segregation using a Darcy-style porous flow, which allowed us to self-consistently generate magma deep in Europa's mantle and then track its evolution in space and time. This approach places physically determined constraints on magma volumes and fluxes available at the base of the brittle silicate lithosphere for subsequent extraction. The newly developed dyke melt-extraction routine then identifies the presence of, and applies two criteria to, melt at the base of a thermally defined lithosphere. For an eruption to occur, (1) the magma must exert sufficient buoyancy stress at the base of the lithosphere to overcome the lithospheric yield stress and initiate a dyke and (2) the dyke must then propagate upward through the lithosphere to the sea floor before conductive cooling solidifies it and arrests its ascent. Our primary finding is that Europa's mantle broadly fails to meet both criteria.

Results

Dyke initiation and tensile strength

First, we evaluated the potential for magma-driven fracturing and dyke initiation at the base of Europa's lithosphere. We treated dyke initiation as a simple contest between magmatic buoyancy-driven stress and the tensile failure strength of Europa's lithosphere. However, it is known that dyke initiation and propagation are driven by a balance of mechanical and fluid stresses, of which magmatic stresses play only a part[26,27]. Despite this, our knowledge of the mechanical elastic and tensile fracturing properties of Europan rock at mantle depths is extremely limited[11]. Even in terrestrial contexts, the tensile strength and fracture toughness of rock is highly uncertain[21], with poor agreement between laboratory studies[28,29] and field estimates at outcrop scale[30,31]. In light of these uncertainties and because our primary focus is on fluid-dynamical processes rather than rock mechanics, we constrained in our model the maximum buoyancy stress that magma generates at the base of Europa's lithosphere (Figs. 2–4 and Table 1) to assess the dyke initiation potential.

In all model cases considered, the magmatic buoyancy stresses generated by the mantle generally range from 1 to 3 MPa. These low stresses stem from a few principal causes. First, the bodies of magma generated in Europa's mantle by our models are generally small and ephemeral. Our model may predict smaller melting and eruption volumes compared with Běhounková et al.[9], probably due to differences between the two melting or tidal heat treatments and domains, even when employing immediate melt extraction. However, we did find agreement with Běhounková et al.[9] regarding where the melt is generated in modern-day Europa. We found that melt in Europa's mantle is generated in a narrow circumferential band around 300–400 km in depth (Fig. 1). This melt is transported up to depths where the temperatures are below the solidus curve, and so it begins to solidify. This freezing precludes the development of long-lived magma bodies of substantial thickness at shallower depths in the Europan mantle and, thus, the build-up of large magma buoyancy stresses at the base of the brittle lithosphere. Additionally, the melt fractions overall are small, generally ranging from 3 to 5%, thus limiting the overall magma volume. Europa's small size also hinders magmatic buoyancy. Its surface gravitational acceleration is ~1.4 m s^{-2} in comparison to Earth's 9.8 m s^{-2}, so that corresponding magma bodies on Earth would generate 10–20 MPa of stress (compared to Europa's 1–3 MPa) and so would be much more able to initiate fractures through which they can ascend than their Europan counterparts.

In light of these results, we conclude that magmatic stresses alone are probably insufficient to overcome the tensile strength of the lithosphere and enable dyking. However, magmatic stresses do not capture the entire relevant stress state when considering magmatic intrusions[26]. First, the tensile strengths of different rocks are difficult to determine experimentally, but they are almost always less than laboratory-measured compressive or shear failure strengths. Typical tensile strengths at similar confining pressures on Earth (at ~20–30 km depth) range from 0.5 to 6 MPa (ref. 32), which are like the buoyancy stresses we found. Commonly, dykes on Earth initiate along pre-existing fracture planes in the rock, sidestepping the need to overcome the undamaged tensile strength[25]. However, the existence of fractures at the base of Europa's lithosphere cannot be assumed, as little work has been done to establish whether they are present.

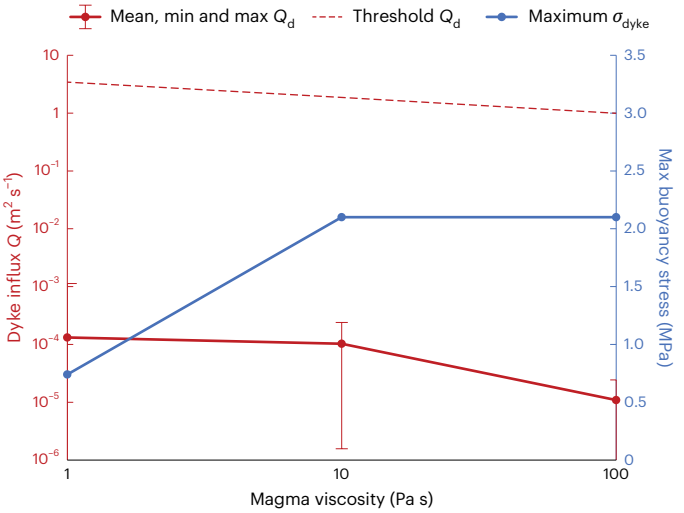

Fig. 2 | The effect of magma viscosity. The mean dyke influx Q_d is the solid red line (left-hand axis). The dyke eruption threshold is the dashed red line (left-hand axis). The maximum magmatic buoyancy stress is the blue line (right-hand axis). Red vertical bars represent the minimum and maximum Q_d in each run, with points representing the mean Q_d over 8,000–15,000 simulated dyke events. When the magma viscosity is increased, the magma velocity into the dyke decreases, reducing Q_d by an equivalent amount. However, more viscous magmas increase the resultant width of the dyke, leading to a decrease in the required eruptive threshold. max, maximum; min, minimum.

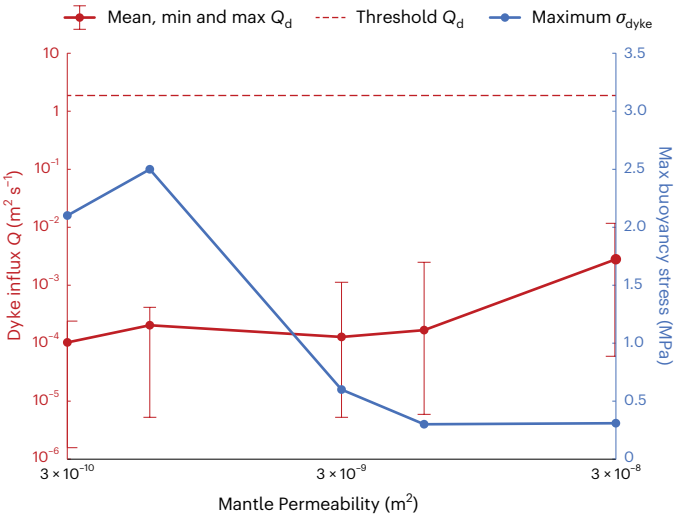

Fig. 3 | The effect of mantle permeability. The mean dyke influx Q_d is the solid red line (left-hand axis). The dyke eruption threshold is the dashed red line (left-hand axis). The maximum magmatic buoyancy stress is the blue line (right-hand axis). Red vertical bars represent the minimum and maximum Q_d in each run, with points representing the mean Q_d over 8,000–15,000 simulated dyke events. Increasing the permeability increases the magma velocity, thus allowing considerably higher dyke influxes. However, a high permeability also prevents the build-up of large bodies of magma, thus decreasing the likelihood of dyke initiation.

https://doi.org/10.1038/s41550-025-02508-8

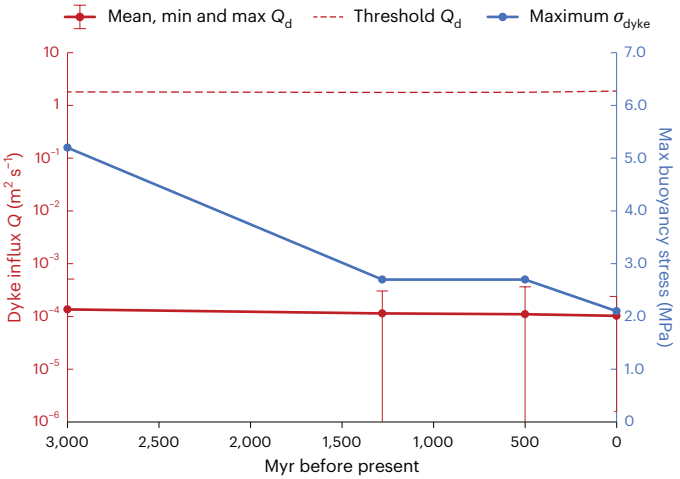

Fig. 4 | The effect of increased radiogenic heat. The mean dyke influx Q_d is the solid red line (left-hand axis). The dyke eruption threshold is the dashed red line (left-hand axis). The maximum magmatic buoyancy stress is the blue line (right-hand axis). Radiogenic heat is presented in millions of years before present and calculated with the radioactive decay equation using the properties of LL chondrites[34]. Red vertical bars represent the minimum and maximum Q_d in each run, with points representing the mean Q_d over 8,000–15,000 simulated dyke events. When the radiogenic heat is increased, we found that, overall, magma production also increases, as reflected by an increase in the maximum magmatic buoyancy stress. However, this does not correspond to an increase in Q_d.

Elastic stresses generated from the melting and subsequent volumetric expansion of mantle rock are also probably present. These stresses are approximately of the order of the magmatic buoyancy stresses found in this study. For example, the partial melting of a 100-km-thick column of rock at 6% will lead to 1% volumetric expansion, which would apply an upward deviatoric stress of 5 MPa to the overlying lithosphere. This value represents a general upper bound on this particular stressor, as 6% melting and a 100-km-tall magma column represent the maximum amount of melting we found in this study during a dyke event. For comparison, for a 2% melt fraction (the average value for a magma body in our reference model), the expansion stress at the base of the lithosphere is only 1.7 MPa.

The Jovian tides exerted on Europa's silicate interior may play a large role in dyke initiation. Tidal loading on lithospheric rock can reduce the tensile strength by up to 33% (ref. 33). Additionally, tidally exerted stresses would probably be additive to magmatic buoyancy stresses during dyke initiation. Yet the stress from the diurnal tide is probably only about 9–13% of the normal fault strength of rocks at Europa's sea floor at a depth of 100 m depth and just 2–3% of that strength at 1 km depth[34] (Supplementary Discussion 2). Diurnal tidal stresses are, thus, unlikely to aid the ascent of magma within Europa's silicate interior, certainly at the depths where melting is occurring. Further work on the stress state of the deep lithosphere informed by our estimates of the limits of magmatic buoyancy is necessary to truly characterize the dyke initiation potential of Europa's mantle, but our overall conclusion that the magma overpressures are insufficient to initiate dyking remains.

Dyke propagation, height and cooling time

Across our models, a brittle lithosphere of 200–250 km thickness develops, which represents the vertical distance a hypothetical dyke must travel for it to erupt at Europa's sea floor. This upwards propagation will be opposed by conductive heat transfer into the surrounding host rock, which will eventually solidify the dyke. In our fluid dynamics treatment of dyke behaviour and propagation, the upwards propagation velocity, along with all other important properties of the dyke, is controlled by the magma influx Q_d (Methods).

To evaluate the propagative and eruptive potential of dykes within Europa's silicate interior, we identified three main model parameters that may impact the fluid dynamic properties of the magma and, therefore, Q_d: the viscosity of the magma (Fig. 2), the permeability of the mantle (Fig. 3) and the amount of radiogenic heat (Fig. 4). We ran alternative models with radiogenic inventories corresponding to those of LL chondrites at 500, 1,280 or 3,000 Myr BP[35] to investigate the effect of increased melt generation and melt volumes on dyke influx. Outside of a supplementary Io case (Supplementary Discussion 3), we did not vary the tidal heat generated because Europa's orbital–tidal evolution was outside the scope of this work (Methods). We varied the viscosity of the magma from 1 to 100 Pa s, capturing a typical range of viscosities for basaltic melt[36]. The melt viscosity plays various roles in controlling melt velocity, dyke influx and dyke half-width, which may have complex effects on the ultimate propagation and height of the dykes (equations (5)–(8)). Finally, we varied the permeability of Europa's mantle k from 3×10^{-10} to 3×10^{-8} m^2. This range falls within (but does not fully capture) the natural variation of permeability for a partially melted peridotitic mantle[37]. Increasing the permeability will increase the melt velocity in the mantle and, therefore, Q_d.

Best-case scenarios for vertical dyke propagation, in which dykes penetrate vertically 1–10 km into the lithosphere, are summarized in Table 1 (see also Supplementary Fig. 6). In most model cases, dykes did not ascend more than 1–2 km into the base of a 200-km-thick lithosphere (that is, ~1% lithospheric penetration). The tallest dyke events occurred in the high-permeability case ($k = 3 \times 10^{-8}$ m^2), reaching a maximum dyke height of 11.5 km (~5% penetration). Importantly, the increased dyke height in this case was accompanied by a 30-km increase in lithospheric thickness relative to the reference model, a perhaps counterintuitive result that is more fully discussed below. This finding means that, although technically the high-permeability cases allow dykes to ascend higher, the lower permeability cases, such as the reference model, feature dykes that reach closer to Europa's sea floor before freezing.

Figures 2–4 show Q_d values as a function of the primary main model parameters controlling dyke height. Dyke influxes average 10^{-4} m^2 s^{-1}, falling approximately five orders of magnitude short of the flux necessary for eruption. For our reference model case, this eruptive threshold (represented by the dashed red lines in Figs. 2–4) is approximately 1.9 m^2 s^{-1} (see Methods for details about this threshold), which is like that for large terrestrial fissure eruptions, such as the Laki eruption in Iceland[38] and in agreement with predicted values from Bland and Elder[11] (~1 m^2 s^{-1}). These low influxes are controlled by the sluggish pore-space flow in the Europan mantle. Very low melt fractions (~3–5%) at the base of the lithosphere strongly hinder the efficient Darcy flow of magma into nascent dykes in addition to the shallow pressure gradients caused by Europa's low gravity. Consequently, the dyke propagation rates were extremely low (~1–3 mm s^{-1}), allowing plenty of opportunity for complete cooling and solidification.

Our variation of magma viscosity (Fig. 2) is reflective of magmas of varying composition that may be present in Europa's mantle, ranging from ultramafic (1 Pa s (ref. 39), which has been identified in Ionian lava flows[40,41]) to high-silica basaltic (100 Pa s)[36]. As the magma viscosity may affect the physical behaviour of the dykes aside from magma velocity alone, we considered the possibility that more viscous magmas are better at propagating dykes upwards than faster moving, less viscous magmas. Table 1 and Fig. 2 demonstrate that this is not the case. A magma viscosity of 100 Pa s will widen the dyke resulting in longer cooling times, in turn leading to a lowering of the threshold Q by a factor of 2 compared with the reference model. However, this lowering is still outpaced by the decrease in dyke influx from the lower magma velocities, which are an order of magnitude lower compared with reference model conditions.

On the other hand, decreasing the magma viscosity hinders dyke propagation more than the resultant increased magma velocities

https://doi.org/10.1038/s41550-025-02508-8

Table 1 | Summary of main results

Model parameter		Avg. Q ($m^2 s^{-1}$)	Max. Q ($m^2 s^{-1}$)	Q threshold ($m^2 s^{-1}$)	σ_{Max} (MPa)	Avg. H_D (km)	Max. H_D (km)	H_L (km)
Reference model		1.03×10^{-4}	2.40×10^{-4}	1.9	2.10	0.64	1.65	196
Radiogenic heat								
Myr BP	**Heat ($W kg^{-1}$)**							
0	5.74×10^{-12}	1.03×10^{-4}	2.40×10^{-4}	1.9	2.10	0.64	1.65	196
500	6.87×10^{-12}	1.10×10^{-4}	3.65×10^{-4}	1.8	2.70	0.74	2.00	202
1,280	9.30×10^{-12}	1.14×10^{-4}	3.04×10^{-4}	1.8	2.70	0.74	1.98	197
3,000	2.02×10^{-11}	1.36×10^{-4}	5.12×10^{-4}	1.9	5.10	0.90	2.39	198
Magma viscosity (Pa s)								
1		1.32×10^{-4}	9.97×10^{-4}	3.4	0.74	0.61	2.79	224
10		1.03×10^{-4}	1.37×10^{-4}	1.9	2.10	0.64	1.65	196
100		1.09×10^{-5}	1.34×10^{-5}	1.0	2.10	0.30	0.83	207
Permeability (m^2)								
3.0×10^{-10}		1.03×10^{-4}	1.37×10^{-4}	1.9	2.10	0.64	1.65	196
6.0×10^{-10}		2.03×10^{-4}	2.12×10^{-4}	1.9	2.50	1.41	2.47	197
3.0×10^{-9}		1.28×10^{-4}	9.93×10^{-4}	1.9	0.60	1.01	3.57	224
6.0×10^{-9}		1.67×10^{-4}	2.04×10^{-3}	1.9	0.30	1.24	5.30	226
6.0×10^{-8}		2.81×10^{-3}	7.73×10^{-3}	1.9	0.31	5.51	11.52	227

The results for the reference model are at the top. Bolded headers separate subsequent model runs by the three main variable parameters considered in this study. Avg., average; H_D, dyke height; H_L, average lithospheric thickness; Q, dyke influx; σ_{Max}, maximum magmatic buoyancy stress.

help. A decreased magma viscosity leads to thinner dykes, which cool faster, increasing the threshold Q from 2 to 3.4 $m^2 s^{-1}$. Lowering the magma viscosity does facilitate the magma pore-space flow, leading to increased average dyke influxes ($Q_d = 1.32 \times 10^{-4}$ $m^2 s^{-1}$) and taller dykes ($H_d = 2.79$ km) overall. However, the faster pore-space flow allows the magma to spread more evenly across the base of the lithosphere than it otherwise would, limiting the build-up of thick, spatially concentrated, intrusive bodies and thus with smaller melt fractions overall (up to 10–100 times less than the reference models; see Supplementary Fig. 7 for a relevant comparison with a high-permeability model). The absence of such large magma bodies serves both to reduce the local buoyancy stress and to lessen the local tidal heating through melt-driven weakening (which plays an important role in warming the lithosphere base and driving further melting). This creates a positive feedback loop of reduced heat and melt generation that serves overall to thicken the lithosphere, which is on average 20 km thicker than the reference model.

We did find, however, that increasing the mantle permeability is an effective method of increasing Q_d. The maximum permeability (3×10^{-8} m^2) that we considered produced an average dyke influx of 2.8×10^{-3} $m^2 s^{-1}$, an order of magnitude greater than the reference model average. However, this flux is still insufficient for eruption by four orders of magnitude. In addition, Fig. 3 shows that this factor of 10 increase in the dyke influx is coupled with a factor of 10 decrease in the magmatic buoyancy stress, as increased melt transport prevents the accumulation of substantial magma volumes at the base of the lithosphere. Additionally, like the reduced viscosity case, increasing the permeability leads to an even thicker lithosphere (30 km thicker than the reference model), which outpaces the increases in dyke height (a maximum of 11 km) by up to a factor of 3. As a result, dyke extraction in a high-permeability mantle is much less probable, despite the increased potential for dyke propagation.

Discussion and conclusions

In addition to the higher radiogenic heat cases shown in Fig. 4, we considered a case with Io-like heat fluxes and found that this model produced eruptions when expected (Supplementary Discussion 3). This Io-like model supports our conclusion that a low melt fraction is the limiting factor for eruptability. We conclude that eruption is possible on Io within this model framework when 'magma mush' conditions (melt fractions of 20–40%) are present at the base of the lithosphere, depending on the grain size of the crystal mush (Supplementary Fig. 8). However, most of the tidal dissipation in Europa probably occurs in its surface ice layer rather than its silicate interior[42], so we do not expect such conditions for Europa. Increasing the radiogenic heat under Europan conditions does not drive a substantial increase in average dyke influx, despite the increase in generated magma volumes because, despite generating melt bodies with fractions of up to 10%, the melt fraction decreases radially outwards from the centre of the body, leaving zones of 2–3% partial melt abutting the lithosphere and the dyke influxes unchanged (Fig. 2).

Our results indicate that a habitable ocean on Europa is unlikely to be presently and solely maintained by sea-floor volcanism. We found that dyke initiation may be challenging at the base of Europa's lithosphere and, if a dyke does form, the magma freezes before it approaches within 150 km of the sea floor, precluding even near-surface hydrothermal alteration driven by plutonic intrusion. However, it is important to note that we tested only one of several possible models of the structure and behaviour of Europa's mantle (Supplementary Discussion 4). Even so, the model presented here was chosen as a particularly optimistic case for the possibility of volcanism, and alternative models, such as those featuring a colder, wetter or undifferentiated interior, will probably be even less able to generate sea-floor volcanism. High-temperature, non-volcanic means of sustaining rock–water reactions, such as serpentinization[8], remain potentially viable. However, our results show that, for thermally driven habitability models or models that rely on passive geochemical exchange with deeper mantle material to be plausible, the lithosphere must be permeable to water all the way through its +200 km depth, as magma will not penetrate beyond the mantle to assist in thermal alteration processes. As low-temperature, non-volcanic, habitability-supporting processes on the sea floor remain plausible, such models of life in Europa's ocean must be considered when assessing Europan habitability.

Methods

The aim of the model was to evaluate the feasibility of Europan sea-floor volcanism by constraining the fluid dynamic behaviour of magma generated in its silicate mantle. To accomplish this, we built a 2D mantle convection and melt transport model in the geodynamic simulation code StagYY, which is fully described by Tackley[25]. Here, we describe the application of StagYY to Europan mantle conditions and the new melt-extraction routine we developed within StagYY. For the Europan ocean to be presently habitable through support from sea-floor volcanism, reductants from volcanic activity and related processes must be periodically released on the sea floor up to and including the present day[1,6,11]. Therefore, the focus of our modelling efforts was to capture the present thermal state of the Europan mantle in the presence of radiogenic heating and tidal dissipation to determine the current likelihood of melt production and resultant melt extraction to the sea floor.

As Europa's mantle is thought to be in the 'cold stagnant lid' tectonic regime[20], we cannot assume that melt-extraction processes associated with plate tectonic activity on Earth apply. Other planets thought to be cold stagnant lids and of similar size to Europa have observable records of volcanism, such as the lunar maria, but those are thought to be ancient and inactive in the present day[43]. Therefore, the hypothetical discovery of similar units on Europa would fail our present-day habitability criteria. Larger planets, such as Venus[44] and Mars[45], have observable records of volcanism into the geologically recent (or even, for Venus, to the present), but their sizes allow for longer-lived and more active mantle dynamics as well as the generation of stable layers of partial melt[46]. The purpose of our mantle model is strictly to supply the new dyke-driven melt-extraction routine with physically constrained present-day magma fluxes, so we did not rigorously consider Europa's secular thermal or orbital evolution here.

To generate a sample of dyke events for analysis, each model was run at steady heat-generation conditions (with no radioactive decay) for 2,000 time steps, which generally corresponds to approximately 200–250 Myr of model time. This runtime was chosen for a few reasons. First, radioactive decay is generally limited over this timescale, and therefore, our choice not to simulate it had a minimal impact. Second, the primary focus of this work is the short-term magmatic processes that occur during dyke-driven volcanism (which occur on timescales of seconds to days) that will be frequently triggered over the considered 200–250 Myr timescale. During a typical model run, 40,000–60,000 individual dyke evaluations were triggered, which allowed a full consideration of both a 'typical' dyke event and all likely possible outliers during a single model run. Therefore, as these models started from a steady-state condition (see below for details) and as the long-term thermal evolution of Europa is not our primary research aim, running models for longer timescales was unnecessary.

Europan mantle model

Our model domain is a 2D spherical annulus[47] 1,421 km in radius with the core–mantle boundary set 600 km above the centre, leading to a mantle layer thickness of 821 km. The model has a resolution of 64 vertical by 512 horizontal cells. The temperatures at the upper and lower boundaries were set to 273 and 1,600 K, respectively. Each model was run from an identical initial condition generated by running a benchmark model with internal heat production and immediate melt extraction matching Běhounková et al.[9] (see details on heat production below) from a preset initial thermal profile of a 'boundary layer' in StagYY to a stable root-mean-square velocity.

Material rheology. We assumed that the rheology of Europa's mantle is dominated by the behaviour of olivine as a typical major constituent of planetary silicate layers, generally the weakest main mineral phase in planetary mantles[48]. In the model, viscosity was treated as Newtonian temperature-dependent diffusion creep due to the low pressures (<4 GPa) and convective stresses (<1 MPa)[9] in the mantle. The material viscosity η was determined in the model with a pressure- and temperature-dependent Arrhenius formulation:

$$\eta(T,p) = A\exp\left(\frac{E+pV}{RT}\right), \quad (1)$$

where T is the material temperature, E is the activation energy, p is the lithostatic pressure, V is the activation volume, R is the ideal gas constant and A is a pre-exponential factor calculated to return the reference viscosity η_0 at temperature T_0. We took $\eta_0 = 10^{18}$ Pa s at $T_0 = T_{CMB} = 1{,}600$ K and varied the viscosity by seven orders of magnitude upwards to a maximum cutoff $\eta_{cutoff} = 10^{25}$ Pa s to allow for a lithosphere of sufficient rigidity while avoiding numerical instabilities caused by extremely large viscosity gradients. Although diffusion creep in olivine is strongly dependent on grain size[49], given that we have virtually no constraints on the grain size in Europa's silicate layer, we did not consider a variable grain size in our viscosity treatment. We chose the most optimistic (the lowest) reference viscosity commonly considered in mantle studies[48], which is representative of smaller grain sizes. Increasing this reference value to incorporate larger grain sizes would, overall, lower the tidal heat production of the layer[42] and, therefore, most probably produce less melt, making volcanism even less probable.

Melting and melt transport. The conservation equations and Darcy flow laws used by StagYY to simulate melt generation and transport are fully described in Hernlund et al.[50] The presence of partial melt in our models reduces the effective viscosity of the host rock as $\eta_{eff} = \eta_s\, e^{-3f_m}$, where η_s is the solid viscosity (equation (1)) and f_m is the melt fraction. We used a dry Herzberg–Boehler solidus[51] to determine the pressure and temperature conditions favourable for melting in the model. Water preferentially partitions into magma when partial melting occurs, so a dry solidus is appropriate, assuming that Europa has experienced previous mantle melting during an era of considerably elevated tidal heating (for example, Hussmann and Spohn[52]) and lacks a mechanism (such as plate tectonics) to reintroduce water into the mantle[9]. When the temperature exceeds the local solidus, melt will be generated and begin to percolate upwards[50]. As it moves upwards, the melt will cool accordingly with the ambient (lower) temperature of the surrounding rock and eventually freeze out, typically at the base of the lithosphere, thus expending its remaining latent heat. This process occurs independently of the dyke melt-extraction process, which is fully described below, and will be superseded if the extraction criteria are met.

Heat production. Heat is produced in the model by both radiogenic activity and tidal flexure. We used the present radiogenic inventory of LL chondrites[35] (the highest heat-producing chondrite class) to account for radiogenic heat production in the mantle. Other chondritic compositions will produce less heat, making volcanism less probable. To achieve a steady state with a constant baseline heat production representative of the conditions today, we ignored radiogenic decay. We added to the radiogenic activity the heat produced by tidal flexure. We simplified tidal heating in comparison to ref. 9, instead using the Maxwell viscosity-dependent treatment of tidal heating by Tobie et al.[42]. Tidal heat production was scaled to the material viscosity by:

$$H_T = \frac{2H_{max}}{\eta(T)/\eta_{max} + \eta_{max}/\eta(T)}, \quad (2)$$

where $\eta_{max} = G/\omega$ represents the material viscosity at which tidal dissipation is at maximum, which is a function of the elastic shear modulus G and Europa's orbital frequency ω. H_{max} represents the maximum tidal dissipation rate at $\eta(T) = \eta_{max}$ and is a function of the elastic properties of the material (G/ω) and the sinusoidal variation in tidal strain rate $\dot{\varepsilon}_{ij}$,

which itself depends on position relative to Jovian tidal force vectors[42]. To capture this spatial dependence, we varied H_{max} positionally along the horizontal θ axis of the model domain:

$$H_{max}(\theta) = \frac{H_{max\_2} - H_{max\_1}}{2} \cos\left[\frac{4\pi}{L_\theta}\left(\theta + \frac{L_\theta}{4}\right)\right] + H_{max\_1}, \quad (3)$$

where L_θ is the domain width, H_{max_1} is the expected lower bound of the tidal dissipation magnitude at the equator and H_{max_2} is the expected upper bound of the tidal dissipation magnitude at the poles. Although these tidal dissipation values have been studied well for Europa's ice[42,53], they are less well constrained for Europa's silicate interior. Tidal heat treatments using a Maxwell rheology may underestimate the total amount of tidal heat produced across the layer by up to a factor of 5 compared with a more rigorous Andrade viscoelasticity treatment[54]. Although implementing a full Andrade-based tidal heat treatment is beyond the current scope of this work, Běhounková et al.[9] used an Andrade-based treatment for tidal heating, which may be approximated through the scaling law we used. Therefore, we empirically determined our chosen values of H_{max_1} and H_{max_2} such that the minimum and maximum amounts of tidal heat generated at the core–mantle boundary matches the tidal heat reported by Běhounková et al.[9] under equivalent conditions for the present (Fig. 1a and Supplementary Table 1). This approach may still underestimate tidal heating in comparison to a full Andrade-based treatment, but it does increase tidal heat output relative to parameters used in a traditional Maxwell tidal heat formulation.

Dyke melt-extraction treatment

We implemented in StagYY a new melt-extraction treatment designed to account for the fluid dynamic limitations of lithospheric melt transport. In this treatment, we conceptualize melt extraction as occurring through the formation and propagation of lithospheric-scale dykes (Supplementary Fig. 5). We define a dyke as a vertically oriented, magma-filled crack with three characteristic dimensions: height, width and breadth. The width of a dyke is generally much smaller (centimetres to metres) than its height and breadth (1 km to hundreds of kilometres), lending dykes a sheet-like appearance when considered in three dimensions (see Rivalta et al.[21] for a full review). In our 2D treatment of dykes, the breadth of a dyke is considered to be orthogonal to the model plane and, therefore, not directly resolved. To erupt, these dykes must initiate above a body of melt pooled at the base of a thermally defined lithosphere and then propagate upward through the entire thickness of the lithosphere. As magma propagates upward, heat is conducted into the host rock, which works to solidify the magma and halt dyke propagation. Bland and Elder[11] developed an analytical treatment of this process, which we adapted for this work. For a discussion of the shortcomings of the modelling approach taken here, we refer the reader to Supplementary Discussion 1.

We used the 'lithosphere' extraction routine in StagYY as the basis for the new dyke extraction treatment. In this melt-extraction routine, two conditions must be satisfied for melt to be extracted: (1) the melt must be in a model cell at the base of the thermal lithosphere, which is defined as the shallowest cell with a temperature $T_L \geq 1{,}400$ K, and (2) the melt within the cell must be positively buoyant throughout the entire thickness of the overlying lithosphere. We chose $T_L = 1{,}400$ K for a few reasons. First, at $T \leq 1{,}400$ K, the rock viscosity is so high that the material does not participate in convective downwellings in the deeper mantle interior, which meets a rheological definition of a lithosphere. Second, at temperatures lower than 1,400 K, the modelled partial melt cools too rapidly to gather at the lithospheric base in substantial amounts, making 1,400 K a natural thermal barrier for aggregating partial melt and the point at which dykes must initiate to continue melt transport. Therefore, if we were to set the temperature higher (for example, 1,500 K), the model would treat cold descending plumes near the core–mantle boundary as if they were lithospheric material, and if we were to set the temperature lower (for example, 1,300 K), the melt would freeze before being accessible to the melt-extraction treatment.

To the above requirements we add two more criteria: (1) magma in the column below the considered cell must exert sufficient buoyancy stress at the lithosphere base to break it and initiate a dyke and (2) the dyke must then propagate upward through the lithosphere faster than conductive cooling can solidify it. We evaluated these two extra criteria through a three-step process (Supplementary Fig. 5).

Step 1: dyke initiation. Once a cell directly above the partial melt that satisfies the original 'lithosphere' criteria has been identified (hereafter referred to as the 'target cell'), we evaluate its ability to initiate a dyke. We adopt a simple 'magma chamber' model (for example, Gudmundsson[32]) in which the primary control of dyke initiation is the non-lithostatic overpressure exerted on the lithosphere by positively buoyant magma. A body of magma will exert a buoyancy stress σ_{dyke} on the overlying lithosphere such that

$$\sigma_{dyke} = \int_{base}^{top} (\rho_s - \rho_m)\, g f_m(i)\, dh, \quad (4)$$

where ρ_s is the density of the solid phase, ρ_m is the density of the melt phase, g is the gravity constant, h is the height of the magma body (discretized into the height of individual cells as dh) and $f_m(i)$ is the melt fraction of each individual cell in the magma column. h was calculated by counting downwards from the target cell until a cell with $f_m = 0$ was reached. We accounted for the melt fraction in each cell when calculating h, as bodies of partial melt will exert less buoyancy stress than a fully molten magma chamber. When σ_{dyke} was calculated, it was compared to the user-defined lithospheric tensile strength σ_{yield}. If $\sigma_{dyke} > \sigma_{yield}$, the dyke was initiated and the routine continued to the dyke propagation step. In this study, we generally set σ_{yield} to an artificially low value such that it was consistently exceeded (for example, 0.1–1 MPa) to allow for a full analysis of dyke propagation.

Step 2: dyke propagation. In our fluid dynamic treatment of dyke propagation, the behaviour of a newly initiated dyke is primarily controlled by the magmatic flux into the dyke Q_d (refs. 11,26). This flux has dimensions of $m^2\ s^{-1}$ and represents the velocity of the magma entering the dyke multiplied by its breadth. As we note above, the breadth of a dyke is not directly resolved in our 2D formulation. Therefore, we assumed that the breadth is limited to the horizontal extent of the magma chamber that the dyke stems from, and that the breadth of this magma chamber in and out of the model plane is approximately equivalent to its thickness. This approach leads to $Q_d = v_m h$, where v_m is the Darcy velocity of the melt in the target cell, as determined by StagYY, and h is the thickness of the magma body already found in the dyke initiation step. Once determined, this Q_d allowed us to compute the upwards propagation velocity v (m s^{-1}; equation (5)) and half-width W (m; equation (6)) of the dyke[11]:

$$v = \left(\frac{Q_d^2 \Delta\rho g}{12\mu}\right)^{1/3}, \quad (5)$$

$$W = \left(\frac{3\mu Q_d}{2\Delta\rho g}\right)^{1/3}, \quad (6)$$

where $\Delta\rho = \rho_s - \rho_m$ and μ is the viscosity of the magma in Pa s.

Step 3: dyke cooling. In fluid dynamic formulations of dyke evolution, dyke growth is limited by the supply and flux of magma into the propagating crack. Therefore, upwards propagation is opposed by the

magma in the dyke conducting heat into the surrounding rock and then cooling and freezing. Once the magma inside freezes, there is no longer a magmatic driving force to propagate the dyke, and it halts. The goal of this step of the model is to determine whether the dyke propagates upwards fast enough to outpace conductive cooling and reach the surface before it solidifies. The cooling time for a dyke in seconds t_c is a function of the dyke half-width, the thermal diffusivity of the host rock κ and a conductive cooling and solidification factor λ:

$$t_c = \frac{W^2}{4\kappa\lambda^2}. \quad (7)$$

λ cannot be solved for analytically and must be numerically approximated with the following transcendental equation:

$$\frac{L\sqrt{\pi}}{c\Delta T} = \frac{e^{-\lambda^2}}{\lambda(1+\mathrm{erf}(\lambda))}, \quad (8)$$

where L is the latent heat of fusion in the magma and c is the specific heat of the host rock. The temperature difference between the liquid and solid phase $\Delta T = T_m - T_s$. The central challenge of approximating λ in this context is finding a reasonable value of ΔT. T_m is held constant at T_L = 1,400 K. However, as a dyke propagates upwards, it will move through the thermal gradient of the lithosphere. Therefore, T_s cannot be held constant, so that magmatic cooling times may vary by up to four orders of magnitude across the ~1,200 K thermal gradient of the lithosphere (Supplementary Table 2).

To account for this, we discretized the lithosphere above the target cell into a 1-km-resolution vertical temperature grid. We then approximated λ to four digits for every value of T_s on the grid and solved individually for t_c. Next, we used the dyke propagation velocity v to calculate the dyke travel time t_z from the point of initiation at the target cell to each point on the grid. If $t_c > t_z$, the dyke propagates upwards faster than it cools and, therefore, moves on to the subsequent grid point. Otherwise, if the dyke takes longer to reach a grid point than it takes to cool at that grid point, the dyke solidifies. We then took the final height of the dyke $d = vt_c$. Finally, we compared d to the thickness of the lithosphere above the target cell z_L. If $d > z_L$, we considered the target cell to be capable of eruption and passed the cell on to the in-built eruption routine in StagYY, which we did not alter for this study.

Calculating the eruptive threshold flux. Additionally, we ran an alternative set of models to determine the threshold magma flux Q_t representative of the minimum magma flux necessary for eruption found in Fig. 3. To find Q_t, in place of the Q calculation described in step 2 above, we assigned to Q_d in the target cell a pseudo-random value in the range 10^{-5} m^2 s^{-1} < Q_d < 10^3 m^2 s^{-1} to capture a broad range of dyke events and behaviours. We then searched for the dyke event that most closely approached $|d - z_L| = 0$ and took the value of Q_d corresponding to that dyke event as the value of Q_t in Fig. 3. Owing to the large number of dyke events triggered in a typical model run, $|d - z_L|$ for each Q_t value presented in Fig. 3 was less than 2 km, with most being less than 500 m. For that reason, and as the absolute lithospheric thickness of each dyke event could vary, this Q_t value should be considered approximate.

Data availability

All data used to generate the results presented in this work and their associated input parameter files are available via Zenodo at https://doi.org/10.5281/zenodo.10850608 (ref. 55).

Code availability

The convection code StagYY is the property of P.J.T. and Eidgenössische Technische Hochschule (ETH) Zürich. Researchers interested in using StagYY should contact P.J.T. (paul.tackley@erdw.ethz.ch).

References

1. Hand K. P. et al. In *Europa* (eds Pappalardo, R. T. et al.) 589–629 (Univ. of Arizona Press, 2009).
2. Vance, S. D. et al. Investigating Europa's habitability with the Europa Clipper. *Space Sci. Rev.* **219**, 81 (2023).
3. Khurana, K. K. et al. Induced magnetic fields as evidence for subsurface oceans in Europa and Callisto. *Nature* **395**, 777–780 (1998).
4. Howell, S. M. The likely thickness of Europa's icy shell. *Planet. Sci. J.* **2**, 129 (2021).
5. Gaidos, E. J., Nealson, K. H. & Kirschvink, J. L. Life in ice-covered oceans. *Science* **284**, 1631–1633 (1999).
6. Chyba, C. F. & Hand, K. P. Life without photosynthesis. *Science* **292**, 2026–2027 (2001).
7. McCollom, T. M. Methanogenesis as a potential source of chemical energy for primary biomass production by autotrophic organisms in hydrothermal systems on Europa. *J. Geophys. Res.: Planets* **104**, 30729–30742 (1999).
8. Vance, S. D., Hand, K. P. & Pappalardo, R. T. Geophysical controls of chemical disequilibria in Europa. *Geophys. Res. Lett.* **43**, 4871–4879 (2016).
9. Běhounková, M. et al. Tidally induced magmatic pulses on the oceanic floor of Jupiter's moon Europa. *Geophys. Res. Lett.* **48**, e2020GL090077 (2021).
10. Trinh, K. T., Bierson, C. J. & O'Rourke, J. G. Slow evolution of Europa's interior: metamorphic ocean origin, delayed metallic core formation, and limited seafloor volcanism. *Sci. Adv.* **9**, eadf3955 (2023).
11. Bland, M. T. & Elder, C. M. Silicate volcanism on Europa's seafloor and implications for habitability. *Geophys. Res. Lett.* **49**, e2021GL096939 (2022).
12. Kattenhorn, S. A. & Prockter, L. M. Evidence for subduction in the ice shell of Europa. *Nat. Geosci.* **7**, 762–767 (2014).
13. Collins, G. C. et al. Episodic plate tectonics on Europa: evidence for widespread patches of mobile-lid behavior in the antijovian hemisphere. *J. Geophys. Res.: Planets* **127**, e2022JE007492 (2022).
14. Greenberg, R. Transport rates of radiolytic substances into Europa's ocean: implications for the potential origin and maintenance of life. *Astrobiology* **10**, 275–283 (2010).
15. Green, A. P., Montesi, L. G. J. & Cooper, C. M. The growth of Europa's icy shell: convection and crystallization. *J. Geophys. Res.: Planets* **126**, e2020JE006677 (2021).
16. Hand, K. P., Sotin, C., Hayes, A. & Coustenis, A. On the habitability and future exploration of ocean worlds. *Space Sci. Rev.* **216**, 95 (2020).
17. Moore, W. B. et al. In *Europa* (eds Pappalardo, R. T. et al.) 369–380 (Univ. of Arizona Press, 2009).
18. Lowell, R. P. & DuBose, M. Hydrothermal systems on Europa. *Geophys. Res. Lett.* https://doi.org/10.1029/2005GL022375 (2005).
19. Moresi, L. & Solomatov, V. Mantle convection with a brittle lithosphere: thoughts on the global tectonic styles of the Earth and Venus. *Geophys. J. Int.* **133**, 669–682 (1998).
20. Weller, M. B. & Lenardic, A. On the evolution of terrestrial planets: bi-stability, stochastic effects, and the non-uniqueness of tectonic states. *Geosci. Front.* **9**, 91–102 (2018).
21. Rivalta, E., Taisne, B., Bunger, A. P. & Katz, R. F. A review of mechanical models of dyke propagation: schools of thought, results and future directions. *Tectonophysics* **638**, 1–42 (2015).
22. Kühn, D. & Dahm, T. Numerical modelling of dyke interaction and its influence on oceanic crust formation. *Tectonophysics* **447**, 53–65 (2008).

23. Lister, J. R. Steady solutions for feeder dykes in a density-stratified lithosphere. *Earth Planet. Sci. Lett.* **107**, 233–242 (1991).
24. Roper, S. M. & Lister, J. R. Buoyancy-driven crack propagation: the limit of large fracture toughness. *J. Fluid Mech.* **580**, 359–380 (2007).
25. Tackley, P. J. Modelling compressible mantle convection with larges viscosity contrasts in a three-dimensional spherical shell using the yin-yang grid. *Phys. Earth Planet. Inter.* **171**, 7–18 (2008).
26. Lister, J. R. & Kerr, R. C. Fluid-mechanical models of crack propagation and their application to magma transport in dykes. *J. Geophys. Res.: Solid Earth* **96**, 10049–10077 (1991).
27. Rubin, A. M. Propagation of magma-filled cracks. *Annu. Rev. Earth Planet. Sci.* **23**, 287–336 (1995).
28. Atkinson, B. K. Subcritical crack growth in geological materials. *J. Geophys. Res.: Solid Earth* **89**, 4077–4114 (1984).
29. Balme, M. R. et al. Fracture toughness measurements on igneous rocks using a high-pressure, high-temperature rock fracture mechanics cell. *J. Volcanol. Geotherm. Res.* **132**, 159–172 (2004).
30. Delaney, P. T. & Pollard, D. D. *Deformation of Host Rocks and Flow of Magma during Growth of Minette Dykes and Breccia-bearing Intrusions near Ship Rock, New Mexico* Professional Paper No. 1202 (USGS, 1981).
31. Scholz, C. H. A note on the scaling relations for opening mode fractures in rock. *J. Struct. Geol.* **32**, 1485–1487 (2010).
32. Gudmundsson, A. Magma chambers: formation, local stresses, excess pressures, and compartments. *J. Volcanol. Geotherm. Res.* **237**, 19–41 (2012).
33. Erarslan, N. & Williams, D. J. Investigating the effect of cyclic loading on the indirect tensile strength of rocks. *Rock Mech. Rock Eng.* **45**, 327–340 (2012).
34. Byrne, P. K. et al. Likely little to no geological activity on the Europan seafloor. In *Proc. 55th Lunar and Planetary Science Conference* https://www.hou.usra.edu/meetings/lpsc2024/pdf/2780.pdf (Lunar and Planetary Institute, 2024).
35. Hussmann, H. et al. Implications of rotation, orbital states, energy sources, and heat transport for internal processes in icy satellites. *Space Sci. Rev.* **153**, 317–348 (2010).
36. Chevrel, M. O., Pinkerton, H. & Harris, A. J. Measuring the viscosity of lava in the field: a review. *Earth-Sci. Rev.* **196**, 102852 (2019).
37. Sundberg, M., Hirth, G. & Kelemen, P. B. Trapped melt in the Josephine peridotite: implications for permeability and melt extraction in the upper mantle. *J. Petrol.* **51**, 185–200 (2010).
38. Thordarson, T. & Self, S. Atmospheric and environmental effects of the 1783–1784 Laki eruption: a review and reassessment. *J. Geophys. Res.: Atmos.* **108**, AAC-7 (2003).
39. Huppert, H. E. & Sparks, R. S. J. Komatiites I: eruption and flow. *J. Petrol.* **26**, 694–725 (1985).
40. Williams, D. A., Wilson, A. H. & Greeley, R. A komatiite analog to potential ultramafic materials on Io. *J. Geophys. Res.: Planets* **105**, 1671–1684 (2000).
41. Williams, D. A., Schenk, P. M. & Radebaugh, J. In *Io: A New View of Jupiter's Moon* (eds Lopes, R. M. C. et al.) 147–172 (Springer, 2023).
42. Tobie, G., Choblet, G. & Sotin, C. Tidally heated convection: constraints on Europa's ice shell thickness. *J. Geophys. Res.* **108**, 5124 (2003).
43. Hiesinger, H. et al. Ages and stratigraphy of lunar mare basalts: a synthesis. In *Recent Advances and Current Research Issues in Lunar Stratigraphy* (eds Ambrose, W. A. & Williams, D. A.) Ch. 1 (Geological Society of America, 2011).
44. Ivanov, M. A. & Head, J. W. The history of volcanism on Venus. *Planet. Space Sci.* **84**, 66–92 (2013).
45. Broquet, A. & Andrews-Hanna, J. C. Geophysical evidence for an active mantle plume underneath Elysium Planitia on Mars. *Nat. Astron.* **7**, 160–169 (2023).
46. Khan, A. et al. Evidence for a liquid silicate layer atop the Martian core. *Nature* **622**, 718–723 (2023).
47. Hernlund, J. W. & Tackley, P. J. Modeling mantle convection in the spherical annulus. *Phys. Earth Planet. Inter.* **171**, 48–54 (2008).
48. Karato, S. *Deformation of Earth Materials: An Introduction to the Rheology of the Solid Earth* (Cambridge Univ. Press, 2008).
49. Hirth, G. & Kohlstedt, D. In *Inside the Subduction Factory. American Geophysical Union, Geophysical Monograph 138* (ed Eiler, J.) 83–106 (American Geophysical Union, 2003).
50. Hernlund, J. W., Tackley, P. J. & Stevenson, D. J. Buoyant melting instabilities beneath extending lithosphere. I. Numerical models. *J. Geophys. Res.* https://doi.org/10.1029/2006JB004862 (2008).
51. Herzberg, C., Raterron, P. & Zhang, J. New experimental observations on the anhydrous solidus for peridotite KLB-1. *Geochem. Geophys. Geosystems* https://doi.org/10.1029/2000GC000089 (2000).
52. Hussman, H. & Spohn, T. Thermal-orbital evolution of Io and Europa. *Icarus* **171**, 391–410 (2004).
53. Ojakangas, G. W. & Stevenson, D. J. Thermal state of an ice shell on Europa. *Icarus* **81**, 220–241 (1989).
54. Bierson, C. J. The impact of rheology model choices on tidal heating studies. *Icarus* **414**, 116026 (2024).
55. Green, A. Repository: no magmatic driving force for Europan seafloor volcanism. *Zenodo* https://doi.org/10.5281/zenodo.10850608 (2024).

Acknowledgements

The research was carried out at the Jet Propulsion Laboratory, California Institute of Technology, under a contract with the National Aeronautics and Space Administration (Grant No. 80NM0018D0004; recipients A.P.G., M.T.B. and C.M.E.). Any use of trade, firm or product names is for descriptive purposes only and does not imply endorsement by the US Government. © 2024. All rights reserved.

Author contributions

A.P.G. led the project; conceptualized, designed and implemented all new additions to StagYY; constructed the Europa interior model; generated all results and wrote the text. C.M.E. and M.T.B. conceptualized the research direction and acquired funding. C.M.E. directly supervised the research and writing process and provided substantial draft revisions. M.T.B. advised on dyke propagation and the acquisition of results and provided substantial draft revisions. P.J.T. advised on model development in StagYY and provided draft revisions. P.K.B. provided substantial draft revisions.

Competing interests

The authors declare no competing interests.

Additional information

Supplementary information The online version contains supplementary material available at https://doi.org/10.1038/s41550-025-02508-8.

Correspondence and requests for materials should be addressed to A. P. Green.

Peer review information *Nature Astronomy* thanks Joseph O'Rourke and the other, anonymous, reviewer(s) for their contribution to the peer review of this work.